EFFECT OF ANNEALING TEMPERATURE ON THE STRUCTURAL AND OPTICAL PROPERTIES OF AL-DOPED ZINC OXIDE (ZnO) CRYSTALS

F.I. EZEMA*, U.O.A. NWANKWO
Department of Physics & Astronomy,University of Nigeria, Nsukka, Enugu State, Nigeria

Aluminium doped zinc oxide (Al-ZnO) crystals have been synthesized via the gel route. Identification of the elemental constituents was carried out using FTIR (Fourier Transform Infra-Red Spectroscopy) analysis. Variation of the structural and optical properties of the crystal with annealing temperature was studied using XRD and UV-VIS techniques respectively. In studying the structural properties, the characteristic (002) plane of ZnO was used as a focal point. Structural analysis showed that the crystal exhibited a preferential growth on the (100), (002) and (101) planes.

(Received September 27, 2010; accepted September 30, 2010)

Keywords: ZnO, Al-doped ZnO crystal; annealing temperature; optical and structural properties

1. Introduction

Zinc Oxide is a wide-band gap group II–VI semiconductor and is typically an n-type semiconductor. In particular, it is considered a promising candidate for use as visible and ultraviolet (UV) light emitters [1]. It exhibits tuneable effect [2] and dopant-related luminescence properties in the visible region of the electromagnetic spectrum. In contrast to gallium nitride (GaN), its main competitor for ultraviolet (UV) applications, ZnO exhibits favourable properties such as a high exciton binding energy of 60 meV (prospect of low laser threshold at room temperature, in contrast to 25 meV for GaN), unproblematic wet-chemical etching, radiation hardness (space applications) and the availability of substrates for homoepitaxy [1]. Zinc oxide is strongly piezoelectric with a coupling factor greater than four times that of quartz [3]. Also, it has a very low dielectric constant making it suitable for such devices as transducers [3]. Crystals of zinc oxide are also useful in acoustical amplifiers, delay lines and other electrical devices.

Various techniques have been employed in the synthesis of doped and undoped zinc oxide crystals. These include sol-gel [4], pulsed laser deposition (PLD) [5], chemical vapour transport [6-9], flux method [10, 11] and hydrothermal method [12, 13]. In this study, we investigate into the effect the increase in the annealing temperature of Al-doped ZnO crystals (grown via the gel route); will have on its structural and optical properties.

2. Experimental details

In the synthesis of aluminium doped zinc oxide crystals, absolute ethanol was used as solvent. Zinc acetate dihydrate [$Zn(CH_3COO)_2 \cdot 2H_2O$] was used as a source of both zinc and oxygen because it is known to be a 'mono-precursor' [14]. This is a unique property of the zinc acetate dihydrate compound. Being a 'mono-precursor' means that one does not need an oxygen precursor to grow ZnO crystals since zinc acetate decomposes to yield zinc oxide. Decomposition of zinc acetate dihydrate to yield zinc oxide proceeds as shown below [14]:

$$4Zn(CH_3COO)_2 \text{ (solid)} \rightarrow Zn_4O(CH_3COO)_6 \text{ (solid)} + (CH_3CO)_2O \text{ (gas)}$$
$$\rightarrow Zn_4O(CH_3COO)_6 \text{ (liquid)}$$
$$\rightarrow 4ZnO \text{ (solid)} + 3CH_3COCH_3 \text{ (gas)} + 3CO_2 \text{ (gas)}$$

It therefore follows that in the use of ethanol as solvent; ethanol could be viewed as being a medium through which heat is supplied for the decomposition of zinc acetate dihydrate. Zinc acetate is known to be soluble in ethanol (and other organic compounds like monoethanolamine, diethanolamine, 2-methoxy ethanol, etc) [15-17].

To synthesize the Al-doped zinc oxide crystals, 10g of Zinc acetate dihydrate [$Zn(CH_3COO)_2{\cdot}2H_2O$] was mixed with 25ml of absolute ethanol (C_2H_5OH) in a beaker. The resulting mixture was stirred using a magnetic stirrer for about 10 minutes after which 0.1g of $AlNO_3$ was added. The mixture was stirred for additional 10 minutes and kept in an oven maintained at 104^{o}C.

After about 120 minutes in the oven, zinc acetate dihydrate and aluminium nitrate decomposed to yield Al-ZnO. Keeping the beaker in the oven (at 104^{o}C) for an additional 90 minutes ensured that the solvent and any moisture present were evaporated completely, leaving behind the Al-ZnO crystals. The crystals were then ground into finer particles using a mortar and pestle.

3. Results and discussion

3.1 FTIR Analysis

FTIR is a technique used to obtain information about the chemical bonding in a material. It is used to identify the elemental constituents of a material sample. FTIR analysis was performed using SHIMADZU FTIR. For our study, the Double-Pass Transmission mode was used. Here, the infrared (IR) beam makes a double pass through the sample before reaching the detector. The double-pass mode was used because it offers the highest level of sensitivity [18].

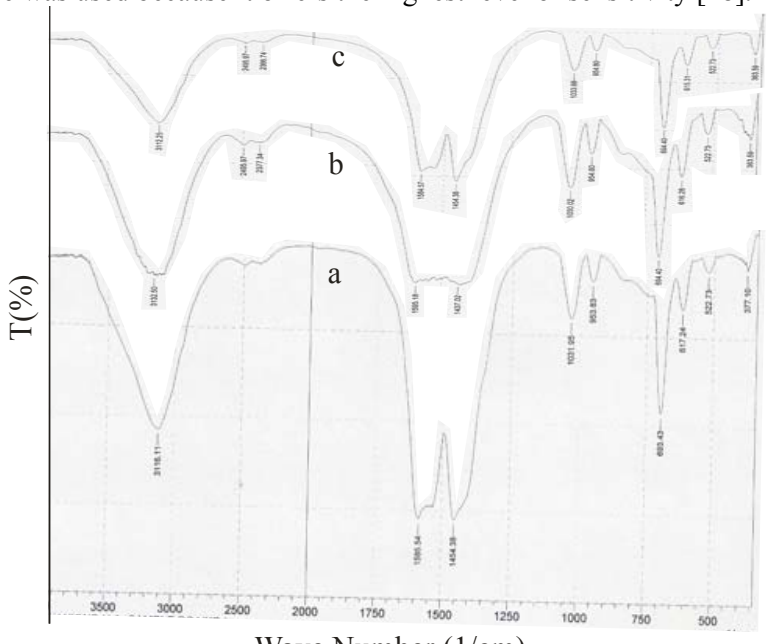

Fig. 1: FTIR Spectra of Al-ZnO crystals – (a) As-grown, (b) Annealed for 10mins at 150^{o}C, (c) Annealed for 10mins at 200^{o}C.

The figure above shows the FTIR spectra of Al-doped ZnO crystal annealed at various temperatures for 10 minutes. In Fig. 1(a), we observe various peaks as indicated, showing the main absorption bands. These absorption bands are due to O-H bending of the hydroxyl group at

1454.38cm^{-1} [19] and O-H out-of-plane bending of the hydroxyl group at 617.24cm^{-1} and 693.43cm^{-1} [19]; O-H stretching of hydroxyl group at 3116.11cm^{-1} [19, 21]; Zn-O stretching of ZnO at 377.10cm^{-1} [20]; and an Al-O stretching at 953.83cm^{-1} [21]. Fig. 1(b) show absorption bands due to O-H bending of the hydroxyl group at 1437.02cm^{-1} [19] and O-H out-of-plane bending of the hydroxyl group at 616.28cm^{-1} and 694.40cm^{-1} [19]; O-H stretching of hydroxyl group at 3132.50cm^{-1} [19, 21]; Zn-O stretching of ZnO at 363.59cm^{-1} [20]; and an Al-O stretching at 954.80cm^{-1} [21]. Similarly, Fig. 1(c) show absorption bands due to O-H bending of the hydroxyl group at 1454.38cm^{-1} [19] and O-H out-of-plane bending of the hydroxyl group at 615.31cm^{-1} and 694.40cm^{-1} [19]; O-H stretching of hydroxyl group at 3112.25cm^{-1} [19, 21]; Zn-O stretching of ZnO at 363.59cm^{-1} [20]; and an Al-O stretching at 954.80cm^{-1} [21].

The presence of the absorption peak associated with the Zn-O and Al-O bonds in each spectra show clearly the presence of zinc oxide and aluminium oxide in the samples. This confirms that the crystal sample analysed is composed of Al-doped zinc oxide crystals.

3.2 Structural analysis

XRD was used to uniquely identify the crystalline phases present in the crystals and to measure the structural properties. The XRD characterisation of crystal samples were carried out using MD-10 Diffractometer. The diffractometer recorded diffractograms using CuK_{α} radiation. Diffraction patterns of the samples were recorded in the 2θ range from 10^{o} to 72^{o}.

The XRD spectra in the figures below show that the compounds grown are crystalline in nature. For each of these XRD spectra, the crystallite size D, was determined using the Debye Scherrer formula [20, 22-24] as given below:

$$D = \frac{K\lambda}{\beta \cos \theta} \tag{1}$$

where K = 0.9, is the shape factor, λ = 1.5408Å, θ is the diffraction peak angle (Bragg Angle) in degrees, and β denotes the full width at half maximum (FWHM) in radians, of the corresponding diffraction peak.

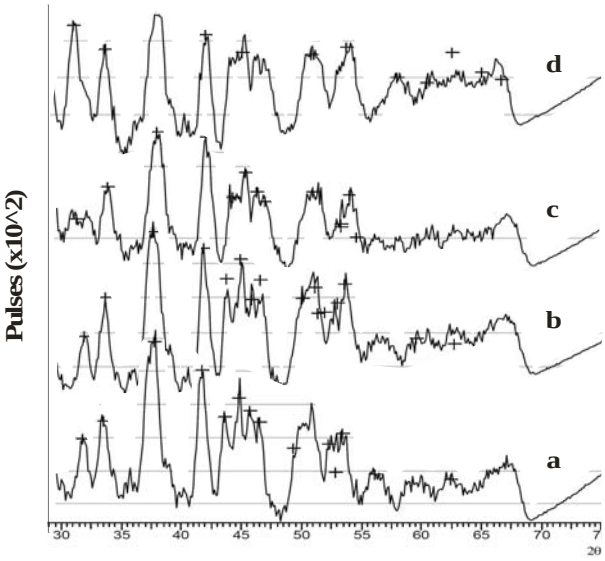

Fig. 2: XRD Spectrum for Al-ZnO crystals – 'a' = As grown, 'b' = Annealed at 100^{o}C for 10 minutes, 'c' = Annealed at 150^{o}C for 10 minutes, 'd' = Annealed at 200^{o}C for 10 minutes

Fig. 2 above shows the XRD spectra of Al-ZnO. Each spectrum in the figure shows that the corresponding crystal sample is crystallized in the wurtzite phase (i.e. has the Zinc Blende wurtzite structure). The peaks in the spectrum in Fig. 2'a' and their corresponding planes are as

follows: (100) for $2\theta^o = 31.79$, (002) for $2\theta^o = 33.48$, (101) for $2\theta^o = 37.69$, (102) for $2\theta^o = 46.48$ and (110) for $2\theta^o = 56.14$. Using the Debye Sherrer formula the crystallite size of the (002) plane [25] was found to be 17.21nm. In Fig 2b, the peaks and their corresponding planes are as follows: (100) for $2\theta^o = 32.0$, (002) for $2\theta^o = 33.76$, (101) for $2\theta^o = 37.75$ and (102) for $2\theta^o = 46.68$. Here, the crystallite size of the (002) plane [25] was found to be 17.68nm. Fig 2c shows the following peaks: (100) for $2\theta^o = 31.29$, (002) for $2\theta^o = 33.83$, (101) for $2\theta^o = 37.96$ and (102) for $2\theta^o = 46.97$. Here, the crystallite size of the (002) plane [25] was found to be 19.88nm. Similarly, in Fig 2d, the peaks and their corresponding planes are as follows: (100) for $2\theta^o = 31.95$, (002) for $2\theta^o = 34.47$ and (101) for $2\theta^o = 38.80$. Here, the crystallite size of the (002) plane [25] was found to be 25.13nm.

The peaks noted above are comparable to the most frequently observed XRD peaks in related studies [24-32]. The (100) peak is labelled as a-axis related and the (002) as the c-axis related [5]. The presence of various peaks corresponding to planes other than the (002) plane shows that samples are polycrystalline in nature [4]. Each XRD spectrum in Fig 2(a-d) shows prominent peaks for the 100, 002 and 101 planes of ZnO, corresponding to the hexagonal wurtzite structure of zinc oxide. These prominent peaks suggest a preferential growth along those planes. We observe that an increase in the annealing temperature of the crystals introduces variations in its structural properties. This variation is shown in table 1, for the (002) plane crystallite size and full width at half maximum (FWHM).

Table 1: Variation of the (002) Plane Crystallite Size and Full Width at Half Maximum (FWHM) of Al-Doped ZnO Crystals with Annealing Temperature.

Sample	Annealing Temperature (^oC)	Crystallite Size (nm)	FWHM (radians)
a	As-grown	17.21	0.96591
b	100	17.68	0.94319
c	150	19.88	0.83979
d	200	25.13	0.66924

Table 1 above shows that increasing the annealing temperature results in Al-ZnO crystals with higher crystallite size and lower widths of the diffraction peak. The higher crystallite size could be attributed to the presence of aluminium ions. Decrease in the width of the diffraction peaks suggests that annealing at higher temperatures produces better quality crystals.

3.3 Optical studies

Optical absorption studies of the crystalline particle colloids were carried out using a JENWAY 6405 UV-VIS spectrophotometer operating at a wavelength range of 200nm to 1200nm at intervals of 5nm. In the optical absorption study, deionised water was used as reference solution [33]. First, the crystal samples were dissolved in deionised water forming a colloidal solution which is then subjected to UV-VIS analysis.

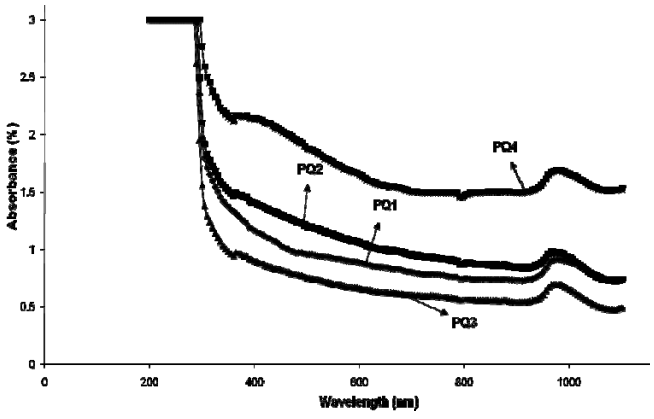

Fig. 3: Optical absorption spectra of Al-ZnO crystals – (PQ1 = As-grown, PQ2 = Annealed for 10mins at 100^{o}C, PQ3 = Annealed for 10mins at 150^{o}C, PQ4 = Annealed for 10mins at 200^{o}C)

The optical absorption spectra above show that annealing Al-ZnO crystals increases its absorbance. The sample annealed at 150^{o}C (PQ3) showed a deviation as it has a lower absorbance compared with others (PQ1, PQ2 and PQ3). The absorption spectrum shows that the crystals have a relatively low absorbance in the visible region, which is a characteristic of ZnO.

Fig. 4 below shows the direct band gap plots. From the figure, PQ1 (as-grown) has a band gap of 3.2eV, PQ2 (annealed for 10mins at 100^{o}C) has a band gap of 3.07eV, PQ3 (annealed for 10mins at 150^{o}C) has a band gap of 3.4eV, while PQ4 (annealed for 10mins at 100^{o}C) has a band gap of 2.95eV. This shows that an increase in the annealing temperature reduces the band gap, though sample PQ3 shows a deviation.

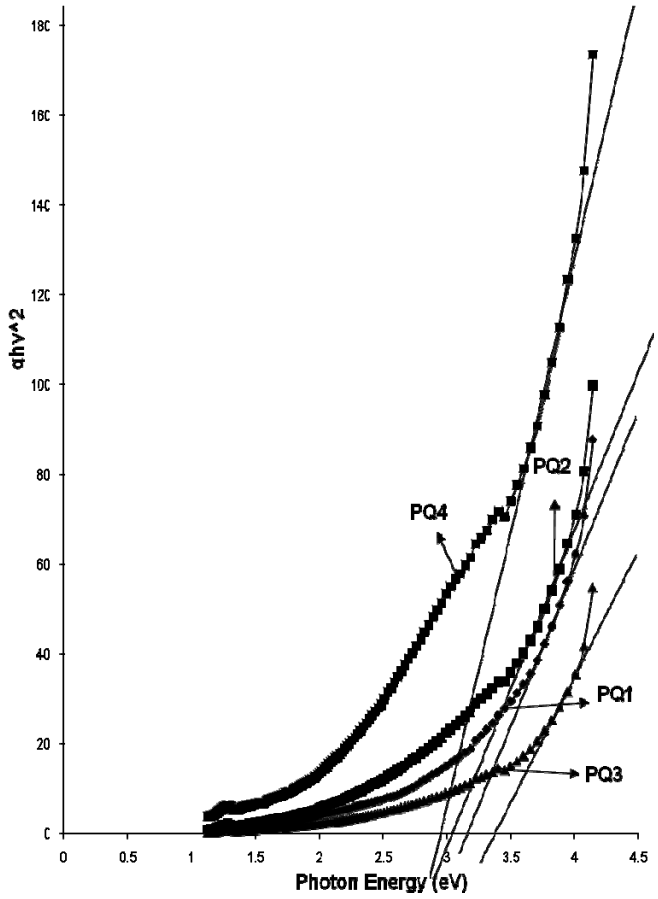

Fig. 4: Plot of Band Gap (Direct) for different annealing temperatures.

The Urbach's energy, which corresponds to the width of the tail of localised states within the optical band gap, is shown in figure 5 below. Urbach's energy can be deduced from the absorption coefficient (α) and depends on structural defects [34]. It is determined by plotting *ln*(α) against photon energy [35], and extrapolating to the photon energy axis. From the figure, Ubarch's energy determined for as-grown Al-ZnO crystals (PQ1) is 0.8eV, for Al-ZnO crystals annealed at 100^{o}C for 10mins (PQ2) is 0.8eV, for Al-ZnO crystals annealed at 150^{o}C for 10mins (PQ3) is 1.1eV, while that for Al-ZnO crystals annealed at 200^{o}C for 10mins (PQ4) is 0.2eV. We observe that the Urbach's energy increases with an increase in annealing temperature. Sample PQ4 showed a drop in the Urbach's energy as compared to sample PQ3. This can be due to the breakdown of crystalline structure of Al-ZnO at high annealing temperature.

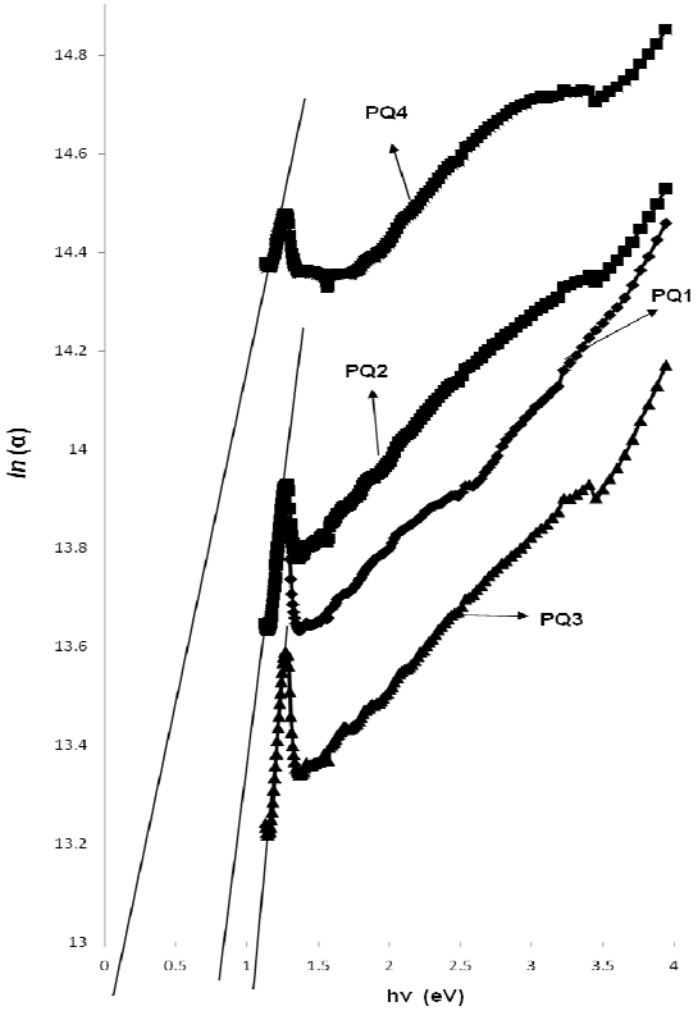

Fig. 5. Urbach's Energy Plot

4. Conclusions

Annealing Al-doped zinc oxide crystals at higher temperatures, results in higher quality crystals. We observe that an increase in the annealing temperature results in an increase in the crystallite size of the (002) plane. This is evident from the crystallite sizes calculated. Also we observe that for the crystals, increase in annealing temperature results in a decrease in the width of the diffraction peak of the (002) plane. This shows that annealing at higher temperatures produces crystals of higher quality. The peaks of the XRD spectra shows that the crystal exhibited preferential growth along the (001), (002) and (101) planes. Optical studies show that subjecting Al-ZnO crystals to increasing annealing temperature increases its absorbance, decreases its band gap (direct) and decreases its Urbach's energy.

References

[1] Grundmann, A. Rahm, T. Nobis, M. Lorenz, C. Czekalla, M.K. Evgeni, J. Lenzner, N. Boukos, A. Travlos, Mohamed Henini (Ed.). Elsevier Ltd. (2008) 293-295.
[2] H. Y. Yang, S.F. Yu, S.P. Lau, Journal of Crystal Growth. **312,** 16 (2009).
[3] J.W. Berry, A.J. Deutschman, United States Patent 3615264. Published 10/26/1971.
[4] P. Sagar, M. Kumar, R.M. Mehra, Materials Science-Poland. **23**(3), 685 (2005).
[5] J.H. Choi, H. Tabata, T. Kawai, J. Crystal Growth. **226**, 493 (2001).
[6] S. Jung, W. Cho, H.J. Lee, M. Oh, Angew. Chem. Int. Ed. 48, 1459 (2009).

[7] D.C. Look, D.C. Reynolds, J.R. Sizelove, R.L. Jones, C.W. Litton, G. Cantwell, W.C. Harsch, Solid State Commun. **105**, 399 (1998).
[8] K. Matsumoto, K. Noda, J. Crystal Growth. **102**, 137 (1990).
[9] J.-M. Ntep, S.S. Hassani, A. Lusson, A. Tromson-Carli, D. Ballutaud, G. Didier, R. Triboulet, J. Crystal Growth. **207**, 30 (1999).
[10] K. Oka, H. Shibata, S. Kashiwaya, J. Crystal Growth **5**, 237 (2002)
[11] N. Ohashi, T. Sekiguchi, K. Aoyama, T. Ohgaki, Y. Terada, I. Sakaguchi, T. Tsurumi, H. Haneda, J. Appl. Phys. **91**, 3658 (2002).
[12] T. Sekiguchi, S. Miyashita, K. Obara, T. Shishido, N. Sakagami, J. Crystal Growth. **214/215** 72 (2000).
[13] T. Sakagami, M. Yamashita, T. Sekiguchi, S. Miyashita, K. Obara, T. Shishido, J. Crystal Growth. **229**, 98 (2001).
[14] A. Wójcik, M. Godlewski1, E. Guziewicz, R. Minikayev, W. Paszkowicz, Journal of Crystal Growth. **310**, 284 (2008).
[15] L. Armelao, M. Fabrizio, S. Gialanella, F. Zordan, Thin Solid Films. **394**, 90 (2001).
[16] H.H. Mohammad, K.S. Mohammad, Journal of Nanomaterials. (2008).
[17] G. Srinivasan, J. Kumar, Cryst. Res. Technol. **41**(9), 893 (2006).
[18] R.C. Brundle, C.A. Evans (Jr.), S. Wilson, Encyclopaedia of Materials Characterization: Surfaces, Interfaces, Thin Films (Materials Characterization Series). Butterworth-Heinemann, Stoneham, MA02180, (1992), 416-427.
[19] J. Coates, Interpretation of Infrared Spectra, A Practical Approach in Encyclopedia of Analytical Chemistry, R.A. Meyers (Ed.), John Wiley & Sons Ltd, Chichester, (2000), 10815–10837.
[20] D. Geetha, T. Thilagavathi, Digest Journal of Nanomaterials and Biostructures. **5**(1), 297 (2010).
[21] K. Nakamoto, Infrared and Raman Spectra of Inorganic and Coordination Compounds, Parts A and B. John Wiley & Sons, New York, (1997).
[22] R. Sharma, B.P. Chandra, D.P. Bisen, Chalcogenide Letters. **6**(8), 339 (2009).
[23] B.E. Waren, X-ray Diffraction, Addison-Wesley, Reading, MA, (1969).
[24] O.W. Perez-Lopez, A.C. Farias, N.R. Marcilio, J.M.C. Bueno, Materials Research Bulletin. **40**, 2089 (2005).
[25] C. Gümüş, O.M. Ozkendir, H. Kavak, Y. Ufuktepe, J. Optoelectron. Adv. Mater. **8**(1),299 (2006).
[26] H. Bahadur, A.K. Srivastava, D. Haranath, H. Chander, A. Basu, S.B. Samanta, K.N. Sood, R. Kishore, R.K. Sharma, Rashmi, V. Bhatt, P. Pal, S. Chandra, Indian Journal of Pure & Applied Physics. **45,** 395 (2007).
[27] N. Singh, S. Mittal, K.N. Sood, Rashmi, R.K. Gupta, Chalcogenide Letters. **7**(4), 297 (2010).
[28] M.W. Cho, C. Harada, H. Suzuki, T. Minegishi, T. Yao, H. Ko, K. Maeda, I. Nikura, Superlattices and Microstructures. **38,** 349 (2005).
[29] R. Thangavel, V. Sabarinathan, S. Ramasamy, J. Kumar, Materials Letters. **61,** 4090 (2007).
[30] M. Wang, S.H. Hahn, J.S. Kim, J. S. Chung, E.J. Kim, K.K. Koo, Journal of Crystal Growth. **310,** 1213 (2008).
[31]E. Suvaci, I.O. Özer, Journal of the European Ceramic Society. **25**, 1663 (2005).
[32] A. Huang, J. Caro, Journal of Crystal Growth. **312**, 947 (2010).
[33] B.S. Amma, K. Manzoor, K. Ramakrishna, M. Pattabi, Materials Chemistry and Physics. **112,** 789 (2008).
[34] S. Tanunchai, S. Towta, N. Mangkorntong, P. Mangkorntong, S. Choopun, Chiang Mai J. Sci. **32**(3), 453 (2005).
[35] R.P. Chahal, S. Mahendia, A.K. Tomar, S. Kumar, Chalcogenide Letters. **7**(8), 569 (2010).